

## Filtration of micron-sized particles in granular media revealed by x-ray computed tomography

F. A. H. Al-Abduwani, R. Farajzadeh, W. M. G. T. van den Broek,  
P. K. Currie, and P. L. J. Zitha<sup>a)</sup>

Department of Applied Earth Sciences, Delft University of Technology, Mijnbouwstraat 120,  
2628 RX Delft, The Netherlands

(Received 10 January 2005; accepted 12 September 2005; published online 19 October 2005)

We investigate the deep-bed filtration of micron-sized hematite particles suspended in distilled water during flow in siliceous granular porous media, where particle retention is mostly due to surface (van der Waals and electrostatic) interactions. We show that x-ray computed tomography enables three-dimensional images of the filtration process to be generated. The one-dimensional filtrate concentration profiles obtained by averaging the images over sections perpendicular to the flow direction are rapidly decaying functions of the distance from the porous medium inlet and slide upward in the course of time, consistently with the filtration model presented by Herzig *et al.* [Ind. Eng. Chem. **62**, 8 (1970)]. Finally, the filtration coefficient is found to decrease rapidly as a function of time: This indicates that the attractive interaction responsible for the retention of the hematite particles is strongly attenuated as the particles accumulate of the pore surfaces. © 2005 American Institute of Physics. [DOI: 10.1063/1.2103467]

### INTRODUCTION

When dilute suspensions of small solid particles are forced through granular porous media, the particles undergo an in-depth filtration process, often referred to as deep-bed filtration.<sup>1–4</sup> This phenomenon is known for a long time and plays an essential role in various applications, including hydrocarbon (oil and gas) recovery,<sup>5</sup> water purification,<sup>6</sup> and environmental protection,<sup>7</sup> to mention only a few. The deep-bed filtration arises from the capture and retention of particles in the pores and involves various elementary mechanisms, of which hydrodynamic transport, mechanical trapping, and surface forces are among the most important.

A considerable number of experimental studies dealing with such processes have been reported in the past few decades, as illustrated in a recent survey by Elimelech *et al.*<sup>6</sup> On the macroscopic level, several phenomenological models have been developed, in the spirit of those presented by Herzig *et al.*<sup>1</sup> Nevertheless, attempts to validate these models using filtration experiments were limited. The available experimental techniques allow only an indirect comparison of the experimental data with the concentration distributions within the porous samples. Kuhnen *et al.*,<sup>7</sup> for instance, used a mathematical inversion analysis of the effluent profiles determined using a light absorption technique. The inversion method is prone to uncertainties, however, and may magnify experimental errors inherent in the determination of the effluent profiles. Locke *et al.*<sup>8</sup> obtained bulk profiles during experiments with sand packs, by sampling the pack at increasing lengths for a given duration of the experiments. This method is both invasive and inaccurate. Ghidaglia *et al.*<sup>9,10</sup>

developed a (refractive) index matched method to visualize the motion of individual particles and study their deposition statistics in glass beads packs. Nevertheless, this technique cannot be used in natural porous media (sand-packs or sandstone) which are opaque. Operating with natural porous samples, Al-Abduwani<sup>11</sup> obtained *in situ* filtration profiles using stereography and chemical analysis after breaking the samples using a three-point bending device at the end of the experiment. However, this technique is also invasive, time consuming, and captures only the end of the experiment. Finally, the determination of filtration parameters from permeability reduction measurements<sup>12</sup> requires the prior knowledge of the relation between permeability reduction and concentration of retained particles.

X-ray computed tomography (CT) enables the visualization of processes within opaque objects by reconstructing the local linear attenuation coefficients from multidirectional x-ray transmission data (see Vinegar and Willington<sup>13</sup>). The purpose of this article is to demonstrate that x-ray computed tomography is a viable technique to obtain three-dimensional pictures of the filtration process inside the porous media. During filtration the attenuation coefficient is modified as a result of the accumulation of retained particles and the CT images represent a three-dimensional mapping of the particle concentration. Linear profiles are generated from the concentration maps to gain more insight into the filtration process. The article continues with a brief review of the filtration theory, the experimental section, and ends with a discussion.

### MODEL

Consider a granular medium with porosity  $\phi$  and mean pore diameter  $d_{po}$ . A dilute suspension of micron-sized particles with mean diameter  $d_{pa}$  is forced through the porous medium at a (superficial) filtration velocity  $u$ . The particles

<sup>a)</sup> Author to whom correspondence should be addressed; electronic mail: p.l.j.zitha@citg.tudelft.nl

are assumed to be very small compared with the pore size, i.e.,  $d_{pa} \ll d_{po}$  and to be retained mainly as a result of to surface interactions (van der Waals or electrostatic). By dilute, it is meant that the average distance between particles  $l$  is much larger than the mean particle diameter, i.e.,  $l \gg d_{pa}$ . This ensures that the interactions between particles are negligible and the contribution of multiparticle bridging to retention can be disregarded. It is further assumed that the suspension is incompressible, gravity effects are negligible, and hydrodynamic dispersion is negligible. Finally, we assume that once retained the particles are not released and that the retained particles hardly change the number of available retention sites. Let now  $c$  be the volume fraction of particles in the suspension and  $\sigma$  the volume fraction of the retained particles with respect to the solid part of the porous medium. In accord with Herzig *et al.*,<sup>1</sup> the filtration can be described by the following system of partial differential equations:

$$\begin{cases} \phi \frac{\partial c}{\partial t} + u \frac{\partial c}{\partial x} = -(1 - \phi) \frac{\partial \sigma}{\partial t}, \\ \frac{\partial \sigma}{\partial t} = \lambda u c \end{cases} \quad (1)$$

where  $\lambda = \lambda(\sigma)$  is a filtration coefficient. The first equation describes the mass conservation of the particles and the second the retention kinetics. The above system of equations can be solved with the initial conditions  $c(x, 0) = 0$ ,  $\sigma(x, 0) = 0$  and the boundary conditions  $c(0, t) = c_0(t)$ . The dependence of the influx concentration on time  $c_0 = c_0(t)$  describes dynamic filtration conditions. Dynamic filtration occurs for instance when there is a buildup of an external filter cake at the inlet face of the porous specimen. Bedrikovetsky *et al.*<sup>12</sup> among others, provided implicit analytical solutions to the problem (1) for arbitrary functions  $\lambda(\sigma)$  and  $c_0(t)$ . When  $\lambda$  and  $c_0$  are assumed to be constant (random particle capture a no buildup of filter cake), such solutions can be given explicitly as

$$\begin{cases} c(x, t) = c_0 \exp(-Kx) \\ \sigma(x, t) = c_0 \phi \lambda_0 (Vt - x) \exp(-Kx) \end{cases} \quad (2)$$

for  $x < Vt$  and  $0$  for  $x \geq Vt$ ,

where  $K = (1 - \phi)\lambda$  and  $V (= u/\phi)$  is the average interstitial velocity. Both the bulk and the retained concentrations  $c(x, t)$  and  $\sigma(x, t)$  have a discontinuity at a moving coordinate  $\xi(t) = Vt$ , which is more visible for small  $K$  (low filtration efficiency). At large  $K$  (high filtration efficiency) the exponential drops rather swiftly, becoming practically zero at  $x = \xi(t)$ , so that the jump is hardly discernible. The bulk concentration  $c(x, t)$  decays according to an enveloping exponential, whereas the filtered concentration  $\sigma(x, t)$  increases linearly with time at any position  $x < \xi(t)$  in addition to the exponential decay. Note that the exponential term in the above solutions is not explicitly dependent on  $V$ , which is a consequence of taking  $\lambda$  constant. The quantity that is of concern in the filtration experiments is the total particle concentration

$$C(x, t) = \phi c(x, t) + (1 - \phi) \sigma(x, t), \quad (3)$$

or, substituting the expression of  $c(x, t)$  and  $\sigma(x, t)$

$$C(x, t) = c_0 \phi [1 + K(Vt - x)] \exp(-Kx). \quad (4)$$

This expression reduces to

$$C_0(t) = c_0 \phi [1 + KVt] \quad (5)$$

for  $x = 0$ . This model represents the minimum description of the deep-bed filtration process, but contains the essential features and is sufficient for the discussion of the experiments that will follow below.

## EXPERIMENT

The x-ray apparatus used in this study is SAMATOM Volume Zoom quad-slice, manufactured by Siemens (Erlangen, Germany) with a spatial resolution  $0.3 \times 0.3 \times 0.5$  mm and temporal resolution of a few seconds per revolution. It is a third generation apparatus in which the x-ray source-detector system rotate continuously for whole object examination using the sequential slicing and spiral methods. The system reconstructs the maps of the linear attenuation coefficients using the SOMARIS SYNGO software. A standalone image processing software was developed in our group for further processing of the data. Adequate precautions were taken to mitigate as much as possible and correct artifacts arising from the scanning and image reconstruction processes.

The quantity provided in the CT images is the local linear attenuation coefficient  $\mu = \mu(x, y, z)$ , which has the units of reciprocal length. The attenuation coefficient depends of the effective density  $\rho$  of the material examined, the atomic number  $Z$ , and the energy  $E$  through the equation

$$\mu = \rho \left( a + b \frac{Z^{3.8}}{E^{3.2}} \right), \quad (6)$$

where  $a$  is the Klein-Nishina cross section and  $b$  a constant ( $= 9.8 \times 10^{24}$  for  $E$  in kilo-electron-volt). The coefficient  $a$  depends slightly on energy but will be taken to be constant in the remainder. The first and second terms in the right-hand side of Eq. (6) describe the Compton scattering and photoelectric absorption, respectively. The former is predominant at high energies ( $E \gg 100$  keV) and the latter at low energies ( $E \ll 100$  keV). Since our CT scanner operates in a nominal range 80–140 keV, both contributions are significant. The effective atomic number  $Z$  is given by the following averaging rule:

$$Z = \left( \sum_i g_i Z_i^{3.8} \right)^{1/3.8}, \quad (7)$$

where  $g_i$  and  $Z_i$  are, respectively, the fraction of electrons and the atomic number of the  $i$ th atomic species. For a dilute suspension in the porous specimen, the effective attenuation coefficient  $\mu$  can be written

$$\mu = \phi \mu_w + (1 - \phi) \mu_s + [\phi c + (1 - \phi) \sigma] \mu_p, \quad (8)$$

where  $\mu_w$ ,  $\mu_s$ , and  $\mu_p$  are the attenuation coefficients of water, solid part of the sandstone (mainly silica), and the particles in suspension. From expression (8) we derive

TABLE I. Properties of the chemical species.

Species	Bulk density	Effective Z	Cross sections <sup>a</sup>	Linear attenuations
	(g/cm <sup>3</sup> )	(-)	(cm <sup>2</sup> /g)	(cm <sup>-1</sup> )
H <sub>2</sub> O	1.0	7.54	0.157	0.1570
SiO <sub>2</sub>	2.7	12.65	0.160	0.4320
α-Fe <sub>2</sub> O <sub>3</sub>	5.4	23.56	0.225	1.215

<sup>a</sup>123 keV, including coherent scattering (Ref. 16).

$$C = \frac{\mu - \mu_r}{\mu_p}, \quad (9)$$

where  $\mu_r$  is the attenuation of the porous specimen saturated with brine only (i.e., for  $c=0$  and  $\sigma=0$ ) and is constant. Recall that the concentration obtained from the CT images using Eq. (9) is a function of the three space variables  $x, y, z$  and time  $t$ . The concentration profiles are obtained by averaging over the slice areas (i.e., over  $x, y$ ). For easy of writing we denote the three-dimensional (3D) and (1D) concentrations using the same symbol  $C$ . Note further that for medical purposes x-ray tomography apparatuses display attenuation coefficients in standardized Hounsfield Units

$$\text{HU} = 10^3 \left( \frac{\mu}{\mu_w} - 1 \right). \quad (10)$$

Clearly for water  $\text{HU}=0$  while for vacuum  $\text{HU}=1000$ . In this study, we convert the HU units into linear attenuation coefficients expressed units of reciprocal length ( $\text{m}^{-1}$ ). This requires the knowledge of the attenuation coefficient of water  $\mu_w$ , which is estimated using the online data base of the National Institute of Standards and Technology (NIST).<sup>16</sup>

The experiments were carried out using nearly homogeneous siliceous porous media (99.2% SiO<sub>2</sub>) and suspension of hematite particles (99.9 Fe<sub>2</sub>O<sub>3</sub>) in double distilled water (99.9% H<sub>2</sub>O). The properties of these materials are given in Table I. The suspension was prepared by adding hematite powder to water under vigorous stirring. The static settling time of the suspension was found to be about five hours. The pH of the suspension was found to be equal to  $6.8 \pm 0.2$ . At this pH value, hematite particles with a point of zero charge (p.z.c.) of 9.0 are positively charged, while the surface of the quartz sandstone is negatively charged (p.z.c.=2.5).<sup>7</sup> Hence, the filtration is controlled by a strong attractive electrostatic interaction. Since hematite particles experience a mutual repulsive force, we expect the filtration to be associated with a monolayer type of retention for which we can use the system of Eqs. (1). To estimate the sensitivity of the CT apparatus for the hematite particles we derive the following expression using Eqs. (9) and (10) using:

$$\Delta C = 10^{-3} \frac{\mu_w}{\mu_p} \Delta \text{HU} \quad (11)$$

and the data in Table I. This expression is derived from Eq. (9) and the definition of HU units given above. The sensitivity the CT scanner is  $\Delta \text{HU}=3$ , hence  $\Delta C=3.87 \times 10^{-4}$ . The porous specimen (diameter= $4.4 \pm 0.1$  cm, length= $18.0 \pm 0.1$  cm, porosity= $22.0\%$ ,  $d_{\text{po}}=12.5 \mu\text{m}$ ) is

held inside a cell made of PEEK (poly-ether-etherketone) using a special glue with a very low penetration at the boundary of the porous medium (see Refs. 14 and 15 for details). PEEK is a special polymeric material which has excellent mechanical properties and is transparent to x rays. The materials used to make the cell (PEEK), and the hardened glue, have two functions: (1) they ensure that the system can withstanding pressures up to 4.0 MPa and temperatures up to 70 °C and (2) since they transmit a narrow x-ray spectrum, they minimize the beam hardening artifact, while providing a good signal-to-noise ratio. The cell with the porous specimen is placed on the couch of the CT scan with its main axis (the flow axis) perpendicular to the scanning plan (x-ray beam plan), to minimize cross artifacts. It is kept in place using a stand equally transparent to x rays.

## DISCUSSION

After an initial scan under dry conditions, the porous sample is saturated with the carrier liquid (double distilled water) and then a new scan is performed. This yields the reference attenuation coefficient  $\mu_r$ . The scanning settings proving the highest signal-to-noise ratio were selected based upon preliminary tests. The suspension, containing particles with a mean diameter  $d_{\text{po}}=12.5 \mu\text{m}$ , with a concentration  $c_0=1.20 \times 10^{-4}$ , is then forced through the porous sample at constant filtration velocity  $u=2.11 \times 10^{-3}$  m/s. This is done using a positive displacement pump. During the injection of the suspension new scans are made at time intervals. The core is scanned perpendicular to its axis producing 80 equally spaced slices, with a thickness of 1 mm.

Figure 1 shows a partial set of images (voxel size:  $0.35 \times 0.35 \times 1.0$  mm) obtained during the above experiment. Each row represents images at different positions for a fixed time while each column represents images of the same slice at different times. In reality, a certain time (about 40 s) is needed to scan the entire porous sample. For this reason, as we shall see below, the scans made at very short times are not very reliable. The attenuation coefficient is given in false color. The distribution of the attenuation coefficients in the images are slightly biased toward the left lower corner due to a small deviation of the axis of the porous sample with respect to the scanning plan. For this reason the images are not totally uniform, contrary to what would be expected from the narrow pore size distribution and neglecting gravity effects. At fixed positions, however (columns in the figure) the buildup of hematite concentration in the porous sample as the filtration progresses is clearly shown by the increase in color intensity as a function of time. The decrease in color intensity with increasing distance, at a fixed time, is a clear manifestation of the filtration process.

For further analysis we construct saturation profiles  $C(x, t)$  using Eq. (9). Figure 2 shows  $C(x, t)$  a function of distance from the inlet, for several times. Note that the  $C(x, t)$  values corresponding to the profile obtained at  $t=60$  s are not very reliable for two reasons: (1) first the amount of retained particles is small and the attenuation is within the sensitivity of the CT apparatus and (2) the scan time is comparable with the elapsed time. For all profiles, the

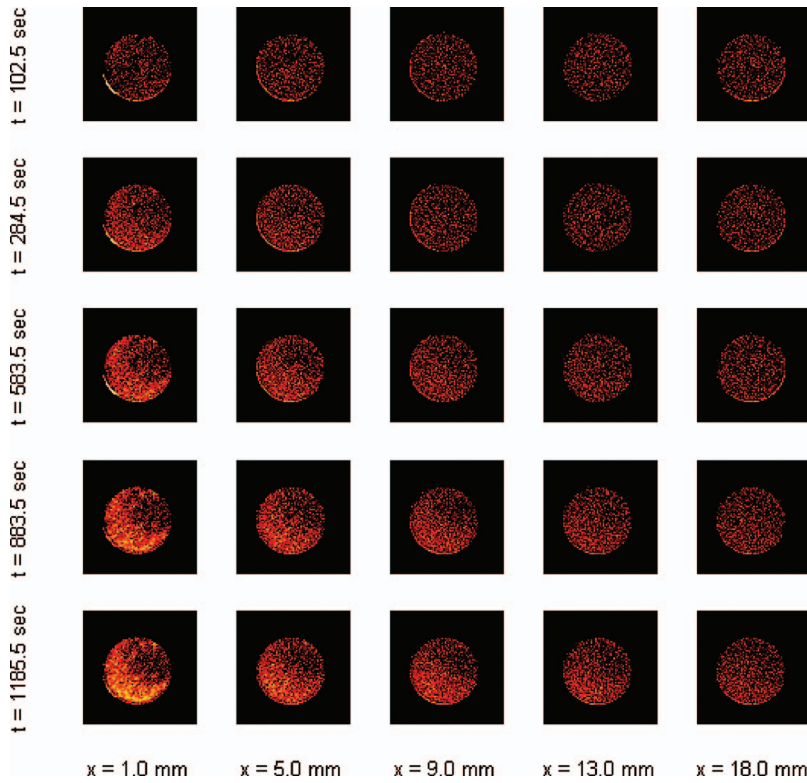


FIG. 1. (Color) Linear attenuation maps obtained by x-ray computed tomography during the flow of suspensions of hematite  $\alpha\text{-Fe}_2\text{O}_3$  ( $c_0=1.2 \times 10^{-5}$ ) in a natural siliceous porous medium ( $\phi=0.22$ ). At a fixed position, the increase in brightness as a function of time,  $x$  (columns), represents the accumulation of hematite particles for the corresponding slice. For fixed times (rows), the decreasing brightness as a function of distance  $x$ , is characteristic of the deep-bed filtration process.

concentration is zero within experimental error beyond a distance of  $x=5$  cm: hence, only data up to this distance will be presented. As has been suggested from the examination of the images in Fig. 1, the concentration profiles decay as a function of  $x$  for a fixed time. From Fig. 2 in can be seen that the profiles are shifted upward for increasing times, in good agreement with Eq. (5). An interesting feature to analyze is the inlet concentration  $C(x,t)$ , which corresponds actually to the first slice of porous medium scanned. In Fig. 3 we have plotted  $C(x,t)$  as a function of  $Vt$ , where the symbols represent the experimental data and the solid line is obtained by

fitting Eq. (5) to the data. From the fitting parameters, we estimated the hematite concentration in the injected fluid and the filtration coefficient, and found:  $c_{0,\text{mes}}=1.22 \pm 0.05 \times 10^{-3}$  and  $K_\infty=0.44 \pm 0.05 \text{ m}^{-1}$  ( $\lambda_\infty=0.56 \pm 0.05 \text{ m}^{-1}$ ), respectively. First of all we remark that  $c_{0,\text{mes}}$  is larger than the nominal injection concentration by an order of magnitude. The reason for this difference and why we use the subscript  $\infty$  will be explained below. First we consider once more the original data and plot  $C(x,t)/C(0,t)$  as shown in Fig. 4. We find that at long times the profiles described by the same master curve (solid line in the graph) satisfying

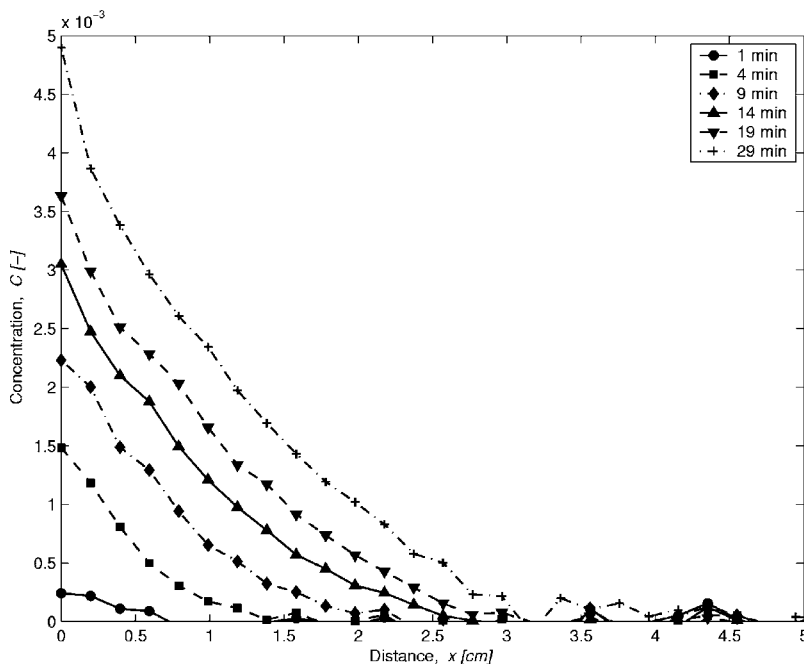


FIG. 2. Concentration of hematite particles  $C(x,t)$  vs distance  $x$ , obtained at various times. The profiles are rapidly decaying functions of  $x$ , and are shifted upward for increasing times, in good qualitative agreement with Eq. (4).

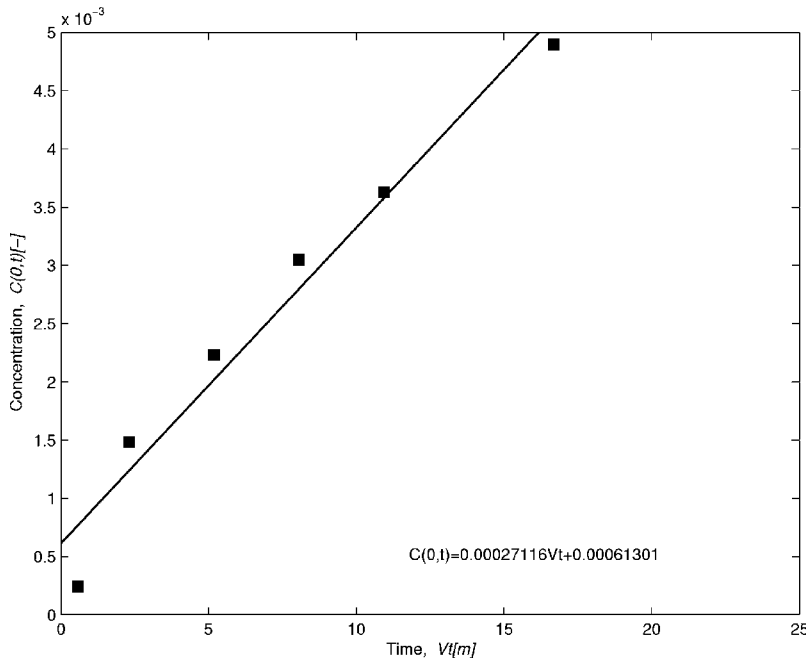


FIG. 3. Concentration of hematite particles in the first slice at the inlet of the porous specimen  $C(0,t)$  vs  $Vt$ : (squares) experimental data and (line) fitting of Eq. (5) to the experimental data. From the fitting parameters we obtain:  $c_{0,mes} = 1.22 \pm 0.01 \times 10^{-4}$  and  $\lambda_\infty = 0.56 \pm 0.05 \text{ m}^{-1}$  is an order of magnitude larger than the injected concentration  $c_0^{mes}$ .

$$\frac{C(x,t)}{C(0,t)} = \exp(-K_0 x), \tag{12}$$

$$C(x,t) = \sigma(x,t) = K_\infty Vt \exp(-K_0 x). \tag{13}$$

where  $K_0 = 0.88 \pm 0.05 \text{ m}^{-1}$  ( $\lambda_0 = 114 \pm 10 \text{ m}^{-1}$ ), qualitatively in good qualitative agreement with Eq. (2). Note that for large  $x$  the data points exhibit a large scatter because, in this case, the measured values of  $C(x,t)$  fall within the sensitivity of the apparatus, and the signal-to-noise ratio is poor. The fact that the experimental data fits the exponential shows that the x-ray computed tomography approach used in this study is a reliable method to estimate concentration changes associated with the filtration phenomenon. However, the fact that  $\lambda_\infty$  is more than two orders of magnitude larger than  $\lambda_0$  implies that the solution (4) of Eq. (1), obtained by assuming that  $\lambda$  is constant is a poor approximation. A better estimate of the concentration profiles is given by

This can be interpreted as follows:  $K_\infty$  reflects the asymptotic behavior of the system at very large  $\sigma$  and  $K_\infty$  at very low values of  $\sigma$ , and consequently  $\lambda$  is a strongly and rapidly decaying function of  $\sigma$ . This can be understood by the following simple physical argument. The hematite particles are positively charged and the surface is initially negatively charged. Therefore a strong attractive interaction favors the capture of the hematite particles. When  $\sigma$  increases, however, the pore surface charge diminishes rapidly in absolute value. This induces a rapid decline of the force responsible for the capture of the particles. This process is likely to stop when  $\sigma$  reaches the value corresponding to a maximum surface coverage. The much larger value of  $c_{0,mes}$ , compared

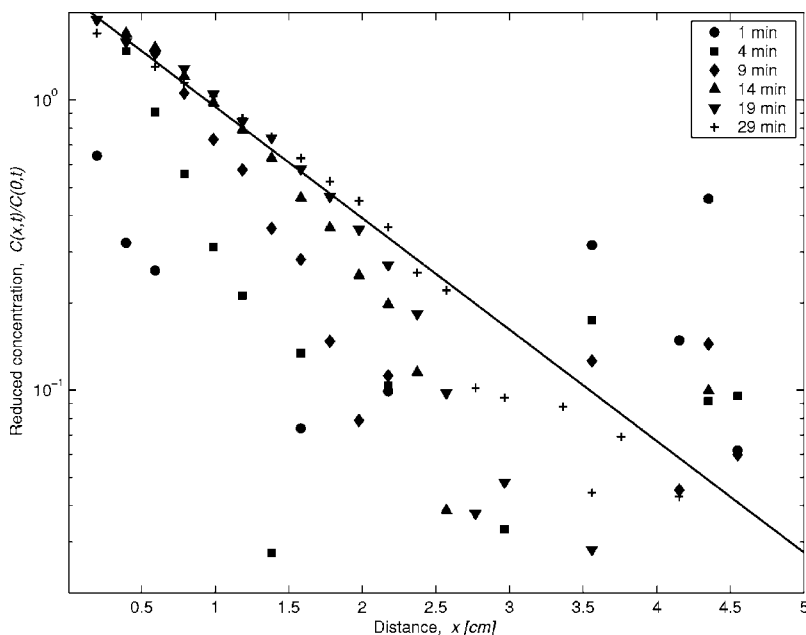


FIG. 4. Semilog plot of the reduced hematite concentration  $C(x,t)/C(0,t)$  vs distance  $x$ . At long times, the experimental data (symbols) fall under the same (master) curve (line) given by  $\exp(-K_0 x)$ , with  $K_0 = 88 \pm 5 \text{ m}^{-1}$ :  $K_0$  is two orders of magnitude larger than  $K_0$ .

with  $c_0$ , indicates that the linear behavior given by Eq. (5) is a good approximation only for large  $\sigma$  (at  $x=0$ ), i.e., for very long times. This is the long time behavior. When  $t$  tends to zero,  $C(0, t)$  is likely to exhibit a much larger slope: but this cannot be confirmed easily, because of the low accuracy of the measurement for low  $\sigma$ .

In conclusion, we have shown that x-ray computer tomography provides *in situ* filtrate concentration distributions resolved in time, during the filtration of colloidal suspensions in granular media. Accurate longitudinal profiles can be obtained more efficiently than with more conventional techniques. Using this approach, we have probed several features of deep bed filtration and have shown that they agree reasonably with the available filtration model, provided that the decline in the filtration coefficient as a function of time is taken into account. Further refinement of this technique should attempt to improve the poor signal-to-noise in the low particle retention region.

## ACKNOWLEDGMENTS

The authors are grateful to Koenraad Elewaut for helping with the computation of the attenuation coefficients. The authors thank Leo Vogt and Adri Maljaars for technical support. The experiments were conducted using the x-ray com-

puter tomography apparatus funded by the Dutch Technology Foundation (STW) through Project No. DAR.5756.

- <sup>1</sup>J. P. Herzig, D. M. Leclerc, and P. LeGoff, *Ind. Eng. Chem.* **62**, 8 (1970).
- <sup>2</sup>L. Lapidus and N. R. Amundson, *J. Phys. Chem.* **56**, 984 (1952).
- <sup>3</sup>H. Soo and C. J. Radke, *Chem. Eng. Sci.* **41**, 263 (1986).
- <sup>4</sup>C. Tien and A. C. Payatakes, *AIChE J.* **25**, 737 (1979).
- <sup>5</sup>F. Civan, *Reservoir Formation Damage: Fundamentals, Modeling, Assessment and Mitigation* (Gulf, Huston, 2000).
- <sup>6</sup>M. Elimelech, J. Gregory, X. Jia, and R. A. Williams, *Particle Deposition and Aggregation; Measurement, Modeling and Simulation* (Butterworth-Heinemann, Oxford, 1995).
- <sup>7</sup>F. Kuhnen, K. Barmettler, S. Bhattacharjee, M. Elimelech, and R. Kretschmar, *J. Colloid Interface Sci.* **231**, 32 (2000).
- <sup>8</sup>M. Locke, B. Indraratna, and G. Adikari, *J. Geotech. Geoenviron. Eng.* **127**, 521 (2001).
- <sup>9</sup>C. Ghidaglia, E. Guazzelli, and L. Oger, *J. Phys. D* **24**, 2111 (1991).
- <sup>10</sup>C. Ghidaglia, L. de Arcangelis, J. Hinch, and E. Guazzelli, *Phys. Rev. E* **53**, R3028 (1996).
- <sup>11</sup>Al-Abduwani (private communication).
- <sup>12</sup>P. Bedrikovetsky, E. Rezende, D. Marchesin, F. Shecaira, A. L. Souza, and P. V. Milanez, *J. Pet. Sci. Eng.* **32**, 167 (2001).
- <sup>13</sup>H. J. Vinegar and S. L. Wellington, *Rev. Sci. Instrum.* **58**, 96 (1986).
- <sup>14</sup>Q. P. Nguyen, Ph.D. dissertation, Delft University of Technology, Delft, The Netherlands (2004).
- <sup>15</sup>P. L. J. Zitha, Q. P. Nguyen, and P. K. Currie (unpublished).
- <sup>16</sup>The cross-sections were estimated from the online Photon Cross Sections Database of NIST, <http://physics.nist.gov/PhysRefData/Xcom/Text/XCOM.html>